Stress gradient effect on the crack nucleation process of a Ti-6Al-4V titanium alloy under fretting loading: comparison between non-local fatigue approaches

Romain Ferré, Siegfried Fouvry, Bruno Berthel, J.-A. Ruiz-Sabariego

Stress gradient effect on the crack nucleation process of a Ti-6Al-4V titanium alloy under fretting loading: comparison between non-local fatigue approaches

R. FERRÉ[1,2)], S. FOUVRY[1)*], B. BERTHEL[1)], J-A. RUIZ-SABARIEGO[2)]

[1)] Laboratoire de Tribologie et Dynamique des Systèmes (LTDS), Ecole Centrale de Lyon, 69134 Ecully cedex, France
[2)] SNECMA Villaroche, SAFRAN group, 77550 Moissy-Cramayel, France

[*]Corresponding author: Tel.: +33 (0)47218 6562; fax: +33 (0)47833 1140.
E-mail address: siegfried.fouvry@ec-lyon.fr

1. Abstract

This study focuses on the stress gradient effect regarding the crack nucleation of a cylinder/plane Ti-6Al-4V titanium alloy contact under low cycle fatigue (LCF) fretting loading. Several local and non-local analytical approaches were compared to predict experimental results. The first part of the study presents fretting nucleation boundaries for three different cylinder radii in the partial slip regime. In the next part, the Crossland and Papadopoulos multi-axial fatigue criteria are computed and compared. Finally, local and non-local fatigue approaches are compared. Square constant volume, critical distance and weighted function approaches have been compared.
The methodology used covers a large range of stress gradients. The impact of varying the stress gradients is that the larger the stress gradient, the larger the difference between experiments and local stress fatigue predictions. A Crossland local form was applied to confirm that a local stress fatigue analysis cannot predict the fretting cracking risk. Three non-local approaches were carried out, and the results allowed the proper prediction of the empirical thresholds with a 3% to 5% margin of error. The positive results obtained helped select a multi-axial fatigue criterion and a non-local approach which take into account the gradient effect of contact fretting behavior.

***Keywords*:** Fretting; Crack nucleation threshold; multi-axial fatigue criterion; Stress gradient effect; Non-local approach

2. Introduction

Fretting is a phenomenon which appears when a contact between two parts is subjected to micro-movements. It is observed in aeronautics, especially in turbojet engines, where high frequency vibrations (some kHz) are combined with cycles of low-frequency fatigue due to repetitive takeoffs and landings. These vibrations induce wear and\or cracking of the interfaces [1]. This type of complex loading can cause a premature breakdown of blade and disk. Ti-6Al-4V titanium alloy, a two-phase alloy, is the material used in the fan stage (blade and disk) of civilian engines [2].

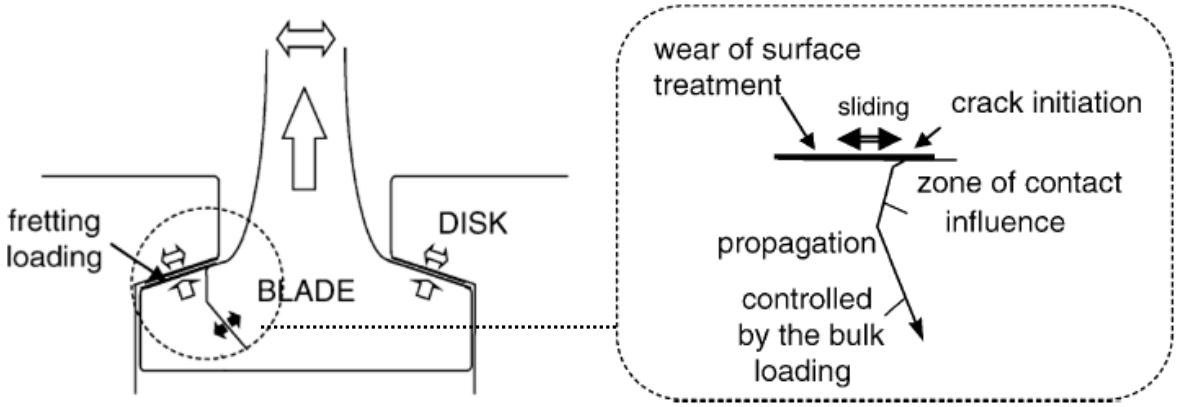

Fig. 1. Illustration of the fretting damage observed in dovetail contacts of turbine engines.

The purpose of this work is to establish a predictive model of cracking nucleation risk under fretting loading in the partial slip regime. The study focuses on the cracking threshold, considering only the effect of the contact radius to optimize the identification of the cracking risk. Stress gradient effects, induced by several contact radii or variable normal pressure levels are analyzed on the cracking threshold. Araújo and al. in [3] performed fretting fatigue experiments with different pad sizes and showed that the lifetime depends on the pad size. Amargier and al. extended this study by working on the effect of pad size and stress gradient on crack initiation. They used a large range of pad sizes in order to cover a large range of stress gradients [4].

Fretting loading induces multiaxial stress fields [5] and severe stress gradients [6]. This multiaxial stress field requires the application of multiaxial fatigue criteria, as discussed in numerous works [7–10]. To optimize the prediction of the cracking risk, "multiaxial criteria" [11, 12] approaches are coupled with "local and non-local" approaches [5, 13–15]. This model has to take into consideration the influence of contact pressure [16] and the stress gradient effect induced by variable radius contacts [4] or variable normal pressure levels. These effects are presented on a single fretting map resulting from experimental tests of a plane/cylinder contact [17]. The representation chosen to compare the different cracking boundaries depending on the various radii and normal pressure levels is a (p_{max} vs. q_{max}) chart introduced in [4].

The method used in this paper neglects wear in the case of partial slip, since cracking process is the predominant damage type observed [3, 5, 15, 18, 19]. The next assumption establishes a transferability of the multiaxial fatigue criteria for high cycle fatigue to the finite endurance condition.

Hence in the first part of this paper, the fatigue limits for a lifetime of 10^5 cycles is determined. Next, the experimental results of fretting tests performed with several cylinder

radii and various normal pressure levels are introduced to highlight the gradient effects. In the subsequent part, two multiaxial fatigue criteria are compared. The first one is the Crossland criterion, which is a tensorial approach using the invariants of the stress tensor's deviator [12]. And the second, from work by Papadopoulos [20], is based on a critical plane approach. Finally, four numerical approaches are studied. A local one, proposed by Petiot [7], is compared with three non-local stress averaging approaches. The first one, presented by Fouvry [21], is based on constant volume with square shape. The second one is the critical distance approach of Araújo's works [22]. The last approach is a weighted function of the equivalent stress field, recently presented in the works of Amargier [4].

3. Studied materials

Fretting tests were performed with specimens made of TA64, which is a two-phase titanium-based alloy. The structure is composed of 60% α phase and 40% of β. The main mechanical properties are displayed in Table 1.

Table 1
Mechanical properties of Ti-6Al-4V

Elastic modulus (GPa)	119
Poisson's ratio	0.29
Yield stress (MPa)	970

Plain fretting loading is cyclic loading. Thus to predict the crack nucleation risk, the fatigue behavior of the alloy studied must be known. Fretting stress is multiaxial, so a multiaxial fatigue criterion approach must be considered. This implies identifying the fatigue behavior under not only tensile but also cyclic shear stress. Note that at the contact border, where the cracking risk is the highest, the loading state alternates. Therefore, both tensile and shear fatigue analyses were performed with a stress ratio R=-1.
First, a global overview of the endurance evolution was described (Fig. 2). Fretting cracking analysis focuses on a 10^5 cycle test duration; therefore, a special attention was taken to identify the tensile and shear fatigue limits at 10^5 cycles by applying the staircase method.

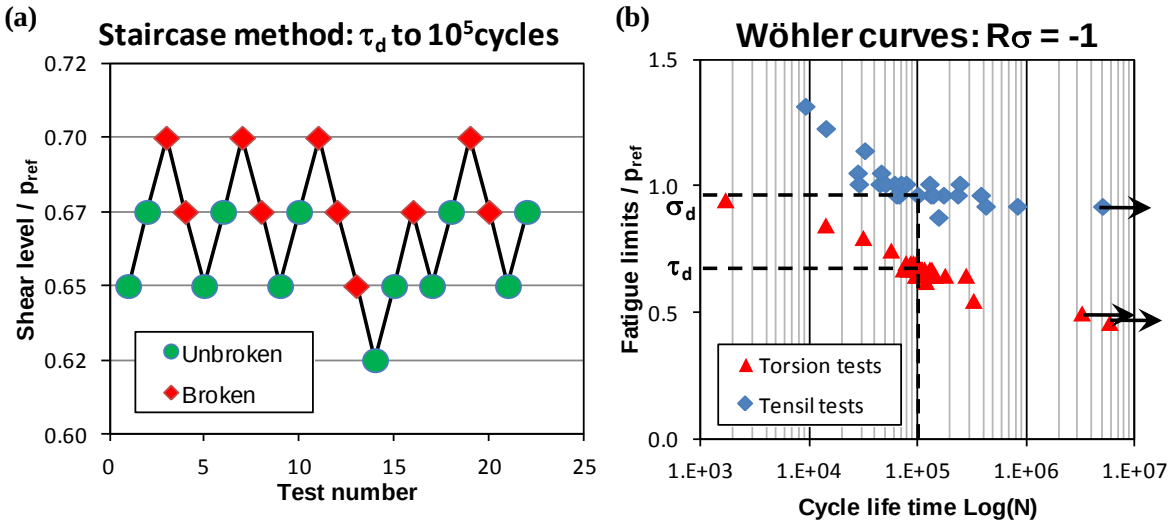

Fig. 2. (a) Staircase levels with broken and unbroken specimens and (b) Wöhler curves with stress ratio R=-1.

Due to confidentiality concerns, the obtained fatigue values are normalized versus a reference maximum Hertzian peak pressure (p_{ref}) used to standardize the analysis of the crack nucleation process in the following investigation. It was found that:

$$\sigma_{-1}(10^5) = 0.97 * p_{ref} \quad (1)$$

$$\tau_{-1}(10^5) = 0.65 * p_{ref} \quad (2)$$

which infers that:

$$\frac{\sigma_{-1}(10^5)}{\tau_{-1}(10^5)} = 1.49 < \sqrt{3} \quad (3)$$

4. Experimental procedure

4.1. Plain fretting test configuration

Plain fretting tests were carried out using a tension-compression MTS hydraulic system [9]. The normal force (P) is kept constant, while the tangential force (Q) and displacement (δ) are recorded. The fretting loop can be plotted and the corresponding amplitude values (respectively Q* and δ*) defined (Fig. 3).
This investigation focuses on the partial slip condition (Q*<μP); therefore, the test was adjusted to impose a constant-tangential-force-amplitude (Q*) loading on a closed fretting loop.

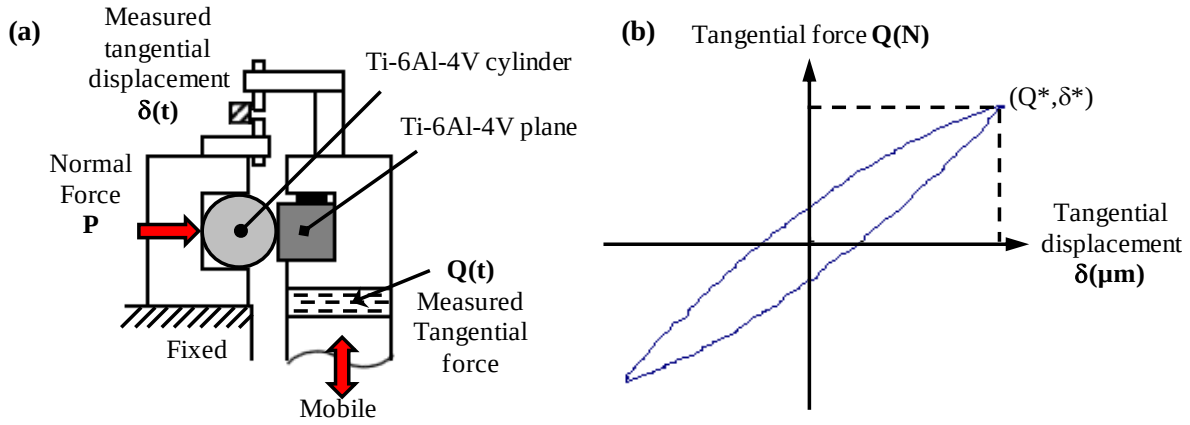

Fig. 3. (a) Schematic of the fretting machine and (b) partial slip fretting cycle.

The number of fretting cycle is set to 10^5cycles and the testing frequency at 10 Hz for this study.

4.2. Contact configurations

Homogeneous cylinder/plane contact configurations were investigated. To standardize the experimental investigations, a reference test condition is considered (R_{ref}, p_{ref}, $qmax_{ref}$). Due to confidentiality issues, this reference condition cannot be provided.
Our objective is to investigate the stress gradient effect; therefore, two other contact radii are investigated ($R_{ref(1/2)}$=1/2*R_{ref} and $R_{ref(2)}$=2*R_{ref}). To maintain a plane strain configuration, the

contact length “L” is adjusted so that the ratio between the contact radius “a” and the contact length is systematically lower than 0.1.

4.3. Definition of the crack nucleation threshold

The cracking investigation consists of identifying the fretting loading inducing a threshold crack length after 10^5 fretting cycles. All stopped tests were investigated with respect to a crack analysis technique inspired by Proudhon and *al.*[23]. The following methodology is applied: After each fretting test, the plane specimen is cut along the median axis of the fretting scar. Gross section observations are performed and not only the real crack length, Lm, but also the projected crack length Lp along the normal of the surface, are measured.
The polishing process is then repeated twice so that the crack measurement is performed on 6 different planes located along the median axis of the fretting scar. From these three measurements, the maximum projected crack length is determined (Lp).
This crack analysis is generalized to various tangential force amplitudes in order to plot the evolution of Lp as a function of the applied tangential force amplitude. As demonstrated in [4], the crack analysis is better formalized using the (p_{max} vs. q_{max}) representation, which is independent of the cylinder radius (Fig. 4).

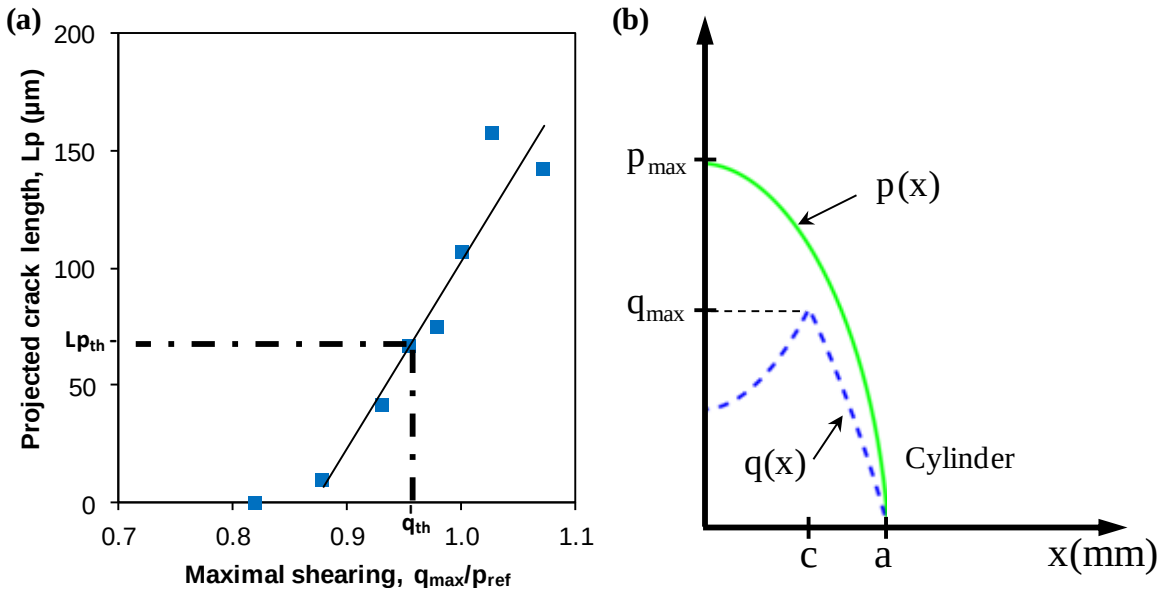

Fig. 4. (a) Evolution of projected crack length Lp as a function of the applied *qmax* value for ($P=P_{ref}$ and $R=R_{ref}$) and (b) normal and tangential stress profiles under fretting contact.

Our crack-nucleation analysis is selected for a structural engineering approach. Therefore, in contrast with conventional analysis, where the crack nucleation threshold is related to a crack length smaller than 10 µm, the given analysis considers a crack length around 70 µm, which is also the smallest crack length which can be detected using potential drop method.
Considering this threshold, Lp_{th}, equal to 70 µm, the corresponding shear fretting loading q_{maxth} is determined. This crack nucleation analysis will be generalized to all the studied fretting loading conditions.

4.4. Analytical computation

The analytical model used in this paper is a two dimensional contact computation. The stress field induced under the surface is fully described by the description of pressure p(x) and shear

q(x) profiles acting on the surface. The partial slip description of the cylinder-plane interfaces studied is addressed using the elastic Mindlin and al. [24] and Cattaneo [25] models. The normal load P and the periodic tangential load Q applied to the bodies (Fig. 3a) impose the elastic stress profiles p(x) and q(x) illustrated in Fig. 4b. The surface tractions p(x) and q(x) are expressed by [26]:

$$p(x) = p_0 \sqrt{1 - \left(\frac{x}{a}\right)^2} \tag{4}$$

$$\frac{q(x)}{\mu p_0} = \begin{cases} \sqrt{1 - \left(\frac{x}{a}\right)^2} - \frac{c}{a}\sqrt{1 - \left(\frac{x}{c}\right)^2} & \left|\frac{x}{c}\right| < 1 \\ \sqrt{1 - \left(\frac{x}{a}\right)^2} & else \end{cases} \tag{5}$$

The contact half-width is defined by a, c is the sticking zone half-width and p_0 is the maximal pressure. Using the equations available in [26], the subsurface stress field can be computed with the previous description of surface tractions. The analytical expressions of the stress tensor elements (σ_{xx}, σ_{zz}, τ_{xz}) are obtained by integrating the complete distributions of p(x) and q(x) over the loaded region. Thus, the stress field can be evaluated for each M(x,z) point in the model.

5. Multiaxial fatigue criteria

Our objective is to predict the crack nucleation risk induced by plain fretting loading under partial slip. The fretting stress field induced by a cylinder/plane contact, in addition to displaying very severe stress gradients, is also multiaxial. Therefore a multiaxial approach will be considered. Two fatigue criteria are examined. The first one, the Crossland criterion, is based on the first invariant, I1, of the stress tensor and the second invariant, J2, of its deviator [27]. The second one, the Papadopoulos criterion, is based on a more physical critical approach. These criteria assume that shear, hydrostatic pressure and its invariants are the parameters that most greatly influence the fatigue life.

5.1. Crossland tensorial approach

One of the most used criteria is called Crossland. It considers $\sqrt{J_{2a}}$, the maximum amplitude of the root square of the deviator second invariant $\sqrt{J_2(t)}$, and the maximum hydrostatic pressure value during the macroscopic loading path, (P_{hmax}), so that there is no cracking risk as long as the following expression is satisfied:

$$\sigma_{eq\_Cross} = \sqrt{J_{2a}} + \alpha_C P_{h\max} < \beta \tag{6}$$

The $\sqrt{J_{2a}}$ variable is given by the following double maximization over the whole loading cycle:

$$\sqrt{J_{2a}} = \frac{1}{2}\max_{t0\in T}\left\{\max_{t\in T}\left[\frac{1}{2}\left(S(t)-S(t_0)\right):\left(S(t)-S(t_0)\right)\right]^{1/2}\right\} \quad (7)$$

where S is the deviator part of the tensor Σ and the symbol " : " expresses the contracted double product. P_{hmax} is defined by the following expression:

$$Ph\max = \max_{t\in T}\left(\frac{1}{3}trace\underline{\underline{\Sigma}}(t)\right) \quad (8)$$

Both α_c and β parameters are functions of the material fatigue properties such that:

$$\beta = \tau_{d-1} \text{ and } \alpha_c = \frac{\tau_{d-1} - \sigma_{d-1}/\sqrt{3}}{\sigma_{d-1}/3} \quad (9)$$

with τ_{d-1} and σ_{d-1}, the fatigue limits under alternated shear and tensile stress conditions, respectively.

5.2. Papadopoulos critical plane approach

The Papadopoulos criterion is an extension of the most common Dang Van's fatigue criterion. Compared to the Dang Van's criterion, the Papadopoulos approach appears better adapted to describing a non-proportional stress field. The formulation of this critical plane approach can be defined as follows: For metals, the elementary volume V is defined as a volume containing a hundred to a thousand grains [28]. It represents the smallest volume that can be considered homogeneous. Assuming a physical point O in the material volume V, we considered a plane, Δ, defined by its normal, n. This vector makes an angle θ with the z-axis of the O_{xyz} frame. The projection of this vector on the xy plane makes an angle φ with the x-axis. For each plane Δ, a quantity called the resolved shear stress is introduced, designated as τa. Papadopoulos introduced a new average value (Formula 10) representing the mean volumetric square root of $Ta(\varphi,\theta,\chi)$ which is defined as follows [11]:

$$\sqrt{\langle\tau_a\rangle^2} = \sqrt{5} * \sqrt{\frac{1}{8\pi^2}\int_{\varphi=0}^{2\pi}\int_{\theta=0}^{\pi}\int_{\chi=0}^{2\pi}\left(\tau_a(\varphi,\theta,\chi)\right)^2 d\chi.\sin\theta.d\theta.d\varphi} \quad (10)$$

The Papadopoulos fatigue criterion is defined as:

$$\sigma_{eq\_Pap} = \sqrt{\langle\tau a\rangle^2} + \alpha_C\sigma_{H,\max} \le \beta \quad (11)$$

As long as this relationship is satisfied, there is no cracking risk.
To define the shear magnitude τa, several steps are necessary. From the previous equations, we can define the six components of the stress tensor stress applied on the right ξ. This tensor is a function of the angles φ, θ, χ and the time t. For a given pair (φ , θ) and a characteristic angle χ of ξ, we can define the resolved shear stress τ acting on Δ along ξ by:

$$\tau_a(\varphi,\theta,\chi) = \frac{1}{2}\left[\max_{t\in P}\tau(\varphi,\theta,\chi,t) - \min_{t\in P}\tau(\varphi,\theta,\chi,t)\right] \qquad (12)$$

The α_c and β material parameters are identical to the ones used in the Crossland expression.

5.3. Finite endurance model

Crossland and Papadopoulos criteria are theoretically related to the fatigue limit conditions. Indeed both the α_c and β material parameters are defined from the tensile and shear fatigue limits at 10^7 cycles ($\tau_{d\text{-}1}$ and $\sigma_{d\text{-}1}$). However, former investigations show that these fatigue criteria can adequately be transposed to the finite endurance domain by considering the corresponding fatigue limit. A similar expression is applied, and the material properties parameters are now expressed by:

$$\beta(N) = \tau(N)_{-1} \text{ and } \alpha(N)_c = \frac{\tau(N)_{-1} - \sigma(N)_{-1}/\sqrt{3}}{\sigma(N)_{-1}/\sqrt{3}} \qquad (13)$$

Fig. 5 plots the evolution of the $\alpha_c(N)$ parameter as a function of the fatigue cycles. The chosen stress ratio $R\sigma$=-1 represents the load ratio imposed at the contact borders of the cylinder/plane fretting tests.

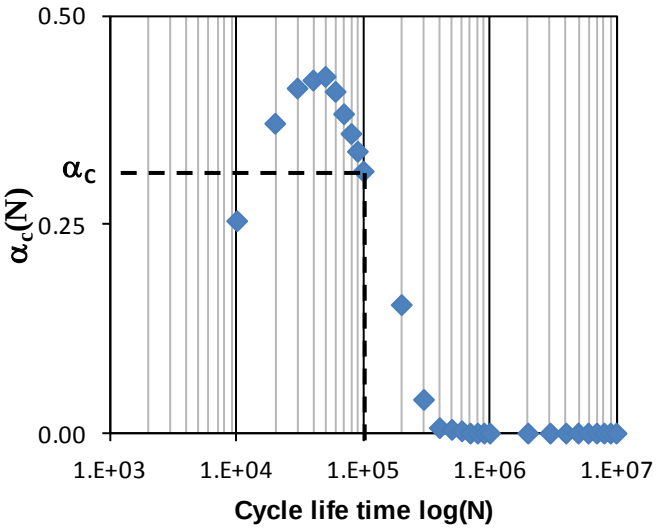

Fig. 5. Evolution of the αc factor versus cycle lifetime N.

An interesting conclusion of this graph is the fact that the $\alpha_c(N)$ parameter is greater than zero in the finite endurance domain ($N < 10^6$ cycles). For instance for the 10^5 cycles test duration, we found $\alpha_c(10^5)$ equals 0.31, which implies that the hydrostatic pressure component for the Crossland criterion or the tensile component for the Papadopoulos criterion will significantly influence the cracking process.

By contrast, for the infinite endurance domain ($N \geq 10^6$ cycles), the $\alpha_c(N)$ parameter converges to zero. This leads to the following important conclusion:

In the infinite endurance domain, because $\alpha_c(N)$ is negligible, the tensile components related to the studied fatigue criterion can be neglected. For the TA64 alloy studied, it can then be concluded that:

If $N \geq 10^6$ cycles (Fatigue limit condition),

Crossland model:

$$\sigma_{eq\_Cross} = \sqrt{J_{2a}} + \alpha_C P_{h\max} = \sqrt{J_{2a}} \tag{14}$$

Papadopoulos model:

$$\sigma_{eq\_Pap} = \sqrt{\langle \pi a \rangle^2} + \alpha_C \sigma_{H,\max} = \sqrt{\langle \pi a \rangle^2} \tag{15}$$

Another interesting conclusion is that if the α_c converges to zero above 5.10^5 cycles this implies that:

$$\tau_{d-1} - \frac{\sigma_{d-1}}{\sqrt{3}} = 0 \tag{16}$$

So that:

$$\tau_d = \frac{\sigma_d}{\sqrt{3}} \tag{17}$$

Finally, from this fatigue investigation, a very basic criterion can be established to define the transition between finite endurance and infinite endurance conditions:

Finite endurance domain: $\alpha_c > 0$ ($N < 10^6$ cycles)
Infinite endurance domain: $\alpha_c = 0$ ($N \geq 10^6$ cycles)

6. Comparison between multiaxial fatigue criteria

The surface distribution of Crossland and Papadopoulos equivalent stresses are compared for the same loading conditions (R_{ref}, p_{ref}, q_{maxref}) in Fig. 6.

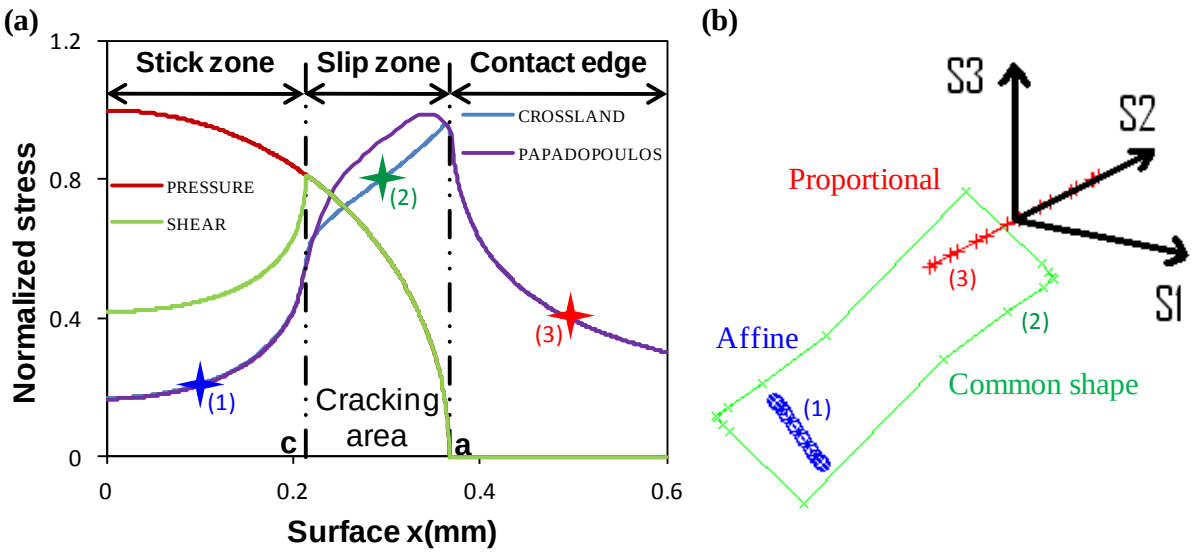

Fig. 6. (a) Stress profiles vs. contact surface and (b) surface loadings in the principal stress frame.

This analysis suggests that the Papadopoulos criterion is more conservative than Crossland's formula. We obtained a 5-percent difference in the maximum equivalent stresses. The second observation is the form of the equivalent stress profiles (Fig. 6a). Both criteria present

equivalent stress values and a similar stress profile in the stick zone at the contact edge. In contrast, in the slip zone, the Crossland criterion displays a linear stress profile with a maximum at "|X| = a". The Papadopoulos criterion displays a convex shape in the external slip area between "c" and "a". The maximum is not located exactly at the contact border but slightly in the sliding zone |X| = 0.95*a. However the difference with the value computed at the contact border (i.e. |X| = a) is very small, which suggests that a Papadopoulos analysis performed at the contact border is quite representative of the maximum cracking risk at the interface.

Another interesting aspect is that the two fatigue models have equivalent results in the stick zone $|X| \leq c$ and outside the contact $|X| \geq a$. Conversely, that of in the sliding zone the Papadopoulos equivalent stress is systematically higher than Crossland. All the criteria lead to a similar prediction at the contact border |X| = a and at the stick boundary |X| = c. To interpret this result, the loading paths computed in three regions (i.e. in the stick zone, sliding zone and outside the contact) are compared.

In the stick zone $|X| \leq c$, the loading path is affine (i.e., linear evolution between stress components). Outside the contact (when |X| > a), the loading path is proportional, which means that in addition to being affine it crosses the origin. The fact that the loading paths in these two domains are affine can explain why similar cracking risks are obtained. Indeed, for this loading path we deduce $\sqrt{\langle \tau a \rangle^2} = \sqrt{J_{2a}}$, which suggests an equivalence between the two equivalent stresses $\sigma_{eq\_Cross} = \sigma_{eq\_Pap}$.

In the sliding zone $c < |X| < a$, the loading path is common and therefore $\sqrt{\langle \tau a \rangle^2} \neq \sqrt{J_{2a}}$. The two criteria lead to different predictions. The averaged variable $\sqrt{\langle \tau a \rangle^2}$ represents the global "shear loading" imposed on the material better than the $\sqrt{J_{2a}}$ variable. Therefore, maximal equivalent stress values of the both criteria are different, and the Papadopoulos criterion becomes more conservative than the Crossland one (i.e., $\max(\sigma_{eq\_Cross}) < \max(\sigma_{eq\_Pap})$).

However our analysis suggests that the maximum cracking risk in the entire interface is well described by the cracking risk computed at the contact border. Therefore, the peculiarity that the loading path is linear and intercepts the origin, can explain why the two criteria lead to equivalent predictions, confirming previous conclusions. To simplify the analysis, the Crossland criterion, which is easier and faster to compute, is preferred. Most of the multiaxial fatigue criteria converge toward the same prediction for collinear fretting fatigue cracking, as was previously highlighted in [29].

7. Crack nucleation analysis

7.1. Influence of the contact stress gradients

The first analysis applied to predict the crack nucleation process consists of considering a local Crossland fatigue stress analysis. The local stress field paths are computed at each point of the planar material during the fretting cycle, and this stress field path is successively transposed to the multiaxial fatigue analysis. Fig. 7 compares the predictions with the obtained experimental results for ($R1=R_{ref(1/2)}$, $R2=R_{ref}$ and $R3=R_{ref(2)}$).

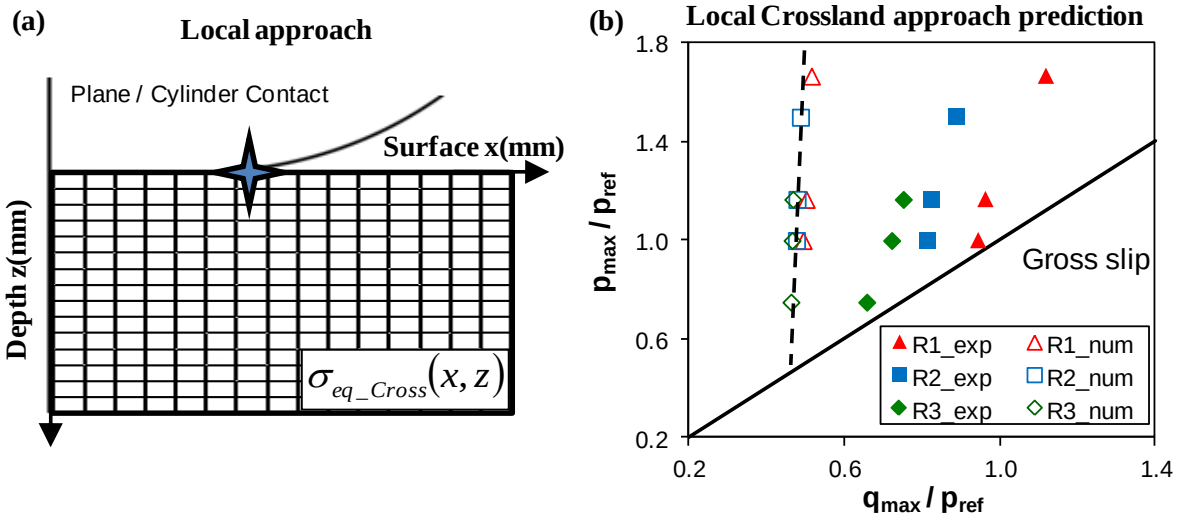

Fig. 7. (a) Numerical local approach scheme and (b) shear threshold predicted by the local approach.

As mentioned by Amargier and al. using (p_{max} vs. q_{max}), the theoretical "local stress" crack nucleation boundary is related to a single master curve independent of the cylinder radius and nearly independent of contact pressure.

Indeed the crack nucleation boundary is related to a threshold $q_{max\_th\_c}$ value. The experimental results display a very different tendency. First, crack nucleation is observed experimentally, for significantly higher shear stress value than predicted, which confirms that the local stress analysis overestimates the cracking risk. Additionally, a pressure dependence of the experimental crack nucleation boundary can be observed. For a given cylinder radius, the higher the contact pressure, the higher the corresponding q_{max} crack nucleation threshold. The larger difference is related to the cylinder size effect. In contrast to the local stress predictions, the experimental crack nucleation boundaries obtained for the various cylinder radii are very different. The smaller the cylinder radius, the larger the q_{max_th} threshold crack nucleation boundary. These typical evolutions can be explained by considering the stress field imposed by the fretting loading.

Fig. 8a compares the evolution of the experimental crack nucleation boundaries obtained for various pressures, on given cylinder radius, with the corresponding stress field computed along the z-axis (i.e., in depth) at the contact border x = a. Whatever the radius, the slopes are always positive and close. This promotes an increase of the cracking threshold as a contact pressure increase:

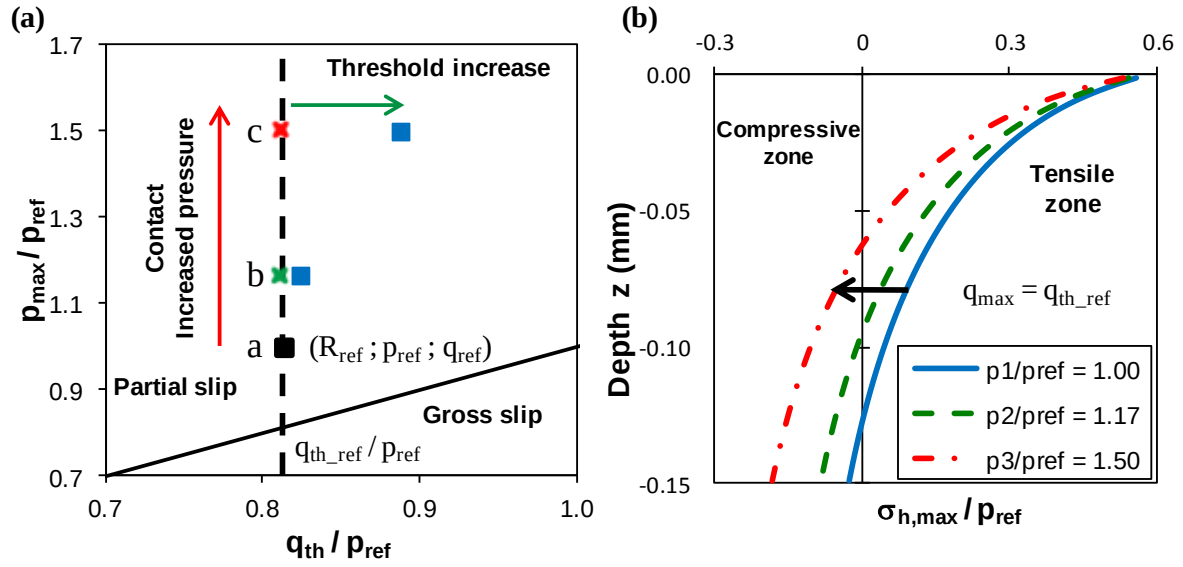

Fig. 8. (a) Contact pressure effect on threshold increase and (b) hydrostatic pressure vs. depth computed at the contact borders below the surface.

Fig. 8b compares the stress fields obtained for a constant q_{max} = q_{th_ref} shear stress field and varying pressure conditions (i.e., points (a, b, c) along the vertical dotted line in Fig. 8a). The "a" condition, corresponds to a crack nucleation condition, whereas the "b" and "c" conditions are far below the crack nucleation condition, although similar q_{max} are imposed. When the contact pressure increases, the hydrostatic pressure converges to the compression domain faster, which indirectly reduces the cracking risk.

To activate the cracking process, higher shear stress fields are consequently required, which explains the shift of the threshold q_{max_th} value observed for the highest pressure conditions. The effect of the cylinder radius and corresponding stress gradient is illustrated in Fig. 9a.

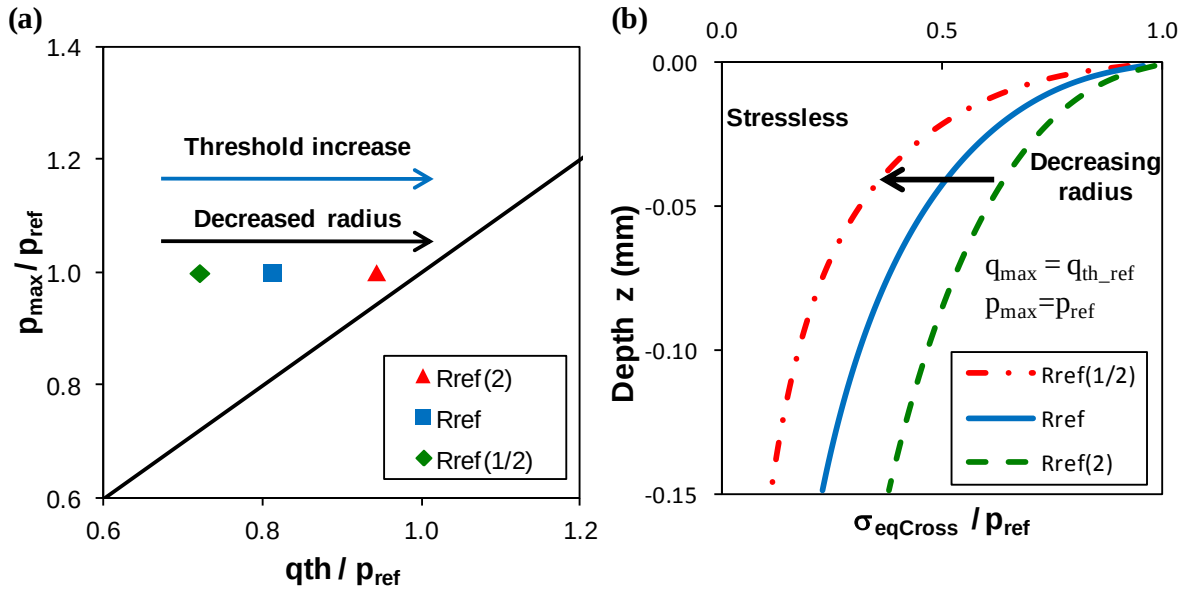

Fig. 9. (a) Gradient effect on crack nucleation boundaries with $R_{ref(2)}<R_{ref}<R_{ref(1/2)}$ and (b) equivalent Crossland stress profiles computed at the contact border along the z-axis for the same p_{ref} and q_{th_ref} but varying cylinder radii

The maximum value of the equivalent Crossland stress at the contact border surface is similar for the three cylinder radii. To interpret the shift of the experimental threshold crack nucleation boundaries, a stress gradient analysis must be considered. The smallest cylinder radius creates the smallest stress gradient beneath the surface. The material volume exposed to the highest stress is consequently very small. In fact, the larger the cylinder radius, the greater the material volume affected by the highest equivalent Crossland stress values. This allows us to explain why the smallest cylinder radius displays the largest threshold q_{th} stress value under equivalent pressure conditions.

7.2. Synthesis

Both contact pressure and cylinder radius analyses demonstrated that to predict the crack nucleation in fretting contact, the influence of the contact stress gradient must be considered. This suggests that an efficient cracking prediction requires non-local fatigue stress analysis. This aspect will be addressed in the following part of this work, focusing on the comparison between different non-local fatigue models currently applied in the fatigue research field and more particularly in notch fatigue failure modeling.

8. Experimental analysis of the cracking process induced by plain fretting loading

8.1. Experimental strategy

The shear threshold values for the Lp_{th} = 70 µm crack nucleation condition have been defined for each contact configuration studied. A major objective of this work is to quantify the effect of the contact stress gradient in the fretting cracking process. Hence various normal forces and cylinder radii have been investigated (Table 2):

Table 2
Maximal shear threshold for various contact radii and contact pressure.

p_{max}/p_{ref}	$R_{ref(1/2)}$	R_{ref}	$R_{ref(2)}$
0.75	-	-	0.66
1.00	0.94	0.81	0.72
1.17	0.97	0.82	0.75
1.50	-	0.89	-
1.67	1.12	-	-

For each studied cylinder radius, $R_{ref(1/2)}$, R_{ref} and $R_{ref(2)}$, contact pressures ranging from $0.75*p_{ref}$ to $1.67*p_{ref}$ have been investigated. A first investigation consists of seeing if the loading conditions related to the crack nucleation process are still elastic. Fig. 10a compares the crack nucleation conditions and the Von Mises boundary in the (p_{max} vs. q_{max}) representation.

Above the threshold Hertzian $p_{0\text{-}H} = 1.6*\sigma y$ value, the maximum plastic deformation is located along the surface. Below $p_{0\text{-}H}$, the maximum plastic deformation is located at the surface in the sliding zone and depends on the shear stress loading. Assuming a local approach, the plastic boundary is related to a constant q_{th} value. Half of the test conditions are located in the elastic zone (i.e., $R_{ref(2)}$ and R_{ref} with $p_{max} < 1.3*p_{th}$), whereas for the smaller cylinder radius, the contact is plastic. However the local stress analysis concerns a very small quantity of material. To be more representative of the global response of the interface, it is more pertinent to consider a non-local plastic approach, by averaging the Von Mises stress

over a grain size volume (Ø = 30 µm). By considering these non-local plastic conditions, the Von Mises boundary shifts to larger shear stress values and displays a similar pressure dependence to that of the local approach.

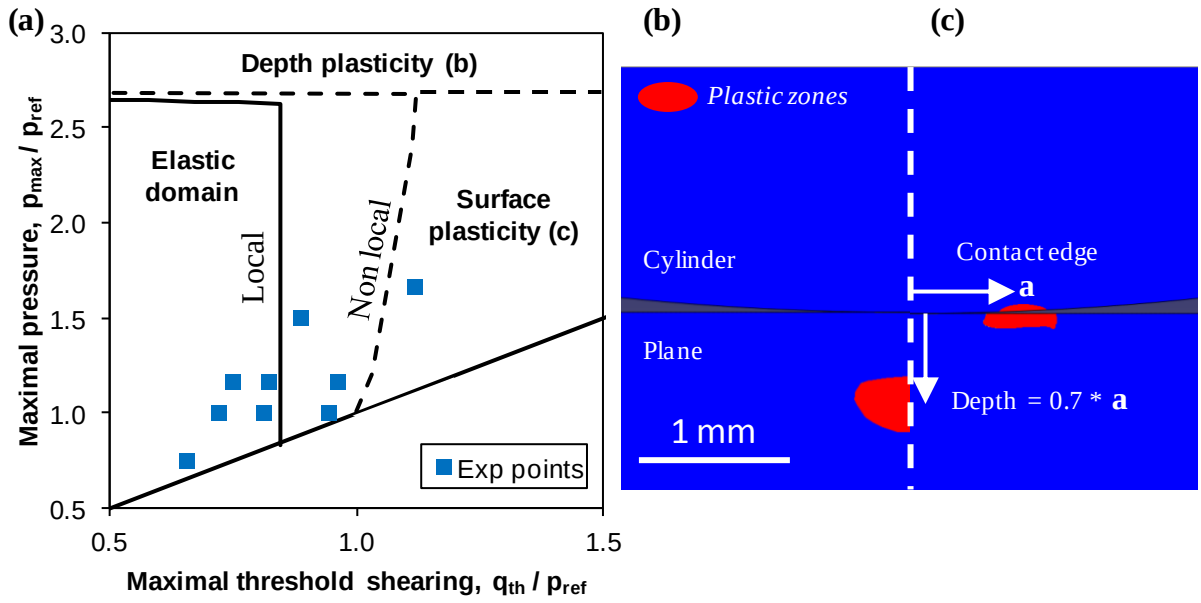

Fig. 10. (a) Von Mises plastic boundary —— local, – – non local: average Von Mises value computed over a 30 µm diameter volume and (b) depth plastic zone and (c) surface plastic localization.

Considering this plastic grain size description, all tested conditions, except the highest pressure situation (1.67*p_{th}, $R_{ref(2)}$), remain in the elastic region. Regarding the material accommodation behavior, it can be assumed that the critical point moves to the elastic domain after some number of fretting cycles. Hence in the following analysis, the contact modeling will be performed by coupling analytical elastic stress descriptions of fretting contacts [30, 31] and multiaxial fatigue criteria.

9. Non local fatigue stress analysis

9.1. Volume averaging stress approach

A first non local approach introduced to predict crack nucleation consists of averaging the equivalent multiaxial criterion over a representative material volume [21]. This approach is currently applied for our 2D contact model, assuming a square surface of width Lv. The Crossland equivalent stress σ_{eq_Cross} is therefore computed for every point, spaced by one micron, using an analytical local stress analysis and successively averaged over the square surface Lv^2.

A first step consists of identifying the Lv parameter. This is obtained by considering the reference conditions (R_{ref}, p_{ref}, $qmax_{ref}$) and adjusting the Lv value until $\sigma_{eq\_Cross}(Lv^2)$ is equal to the crack nucleation condition.

$$\sigma_{eq\_Cross}(Lv^2) = \tau_{d\_10^5} \qquad (18)$$

This analysis leads to Lv = 37 µm, which is very close to the one previously extracted for high cycle fretting conditions (10^6 cycles) [2]. The parameter Lv is maintained constant and applied for the other threshold crack nucleation conditions. Fig. 11 compares the experimental

(p_{max} vs. q_{max}) crack nucleation conditions with the given prediction. The correlation is very good. It is interesting to see that this very basic non-local approach, which is very easy to transpose in Finite Element Modeling simulations (i.e., optimization of the mesh dimensions), is suitable to describe not only the pressure but also the cylinder radius effects.

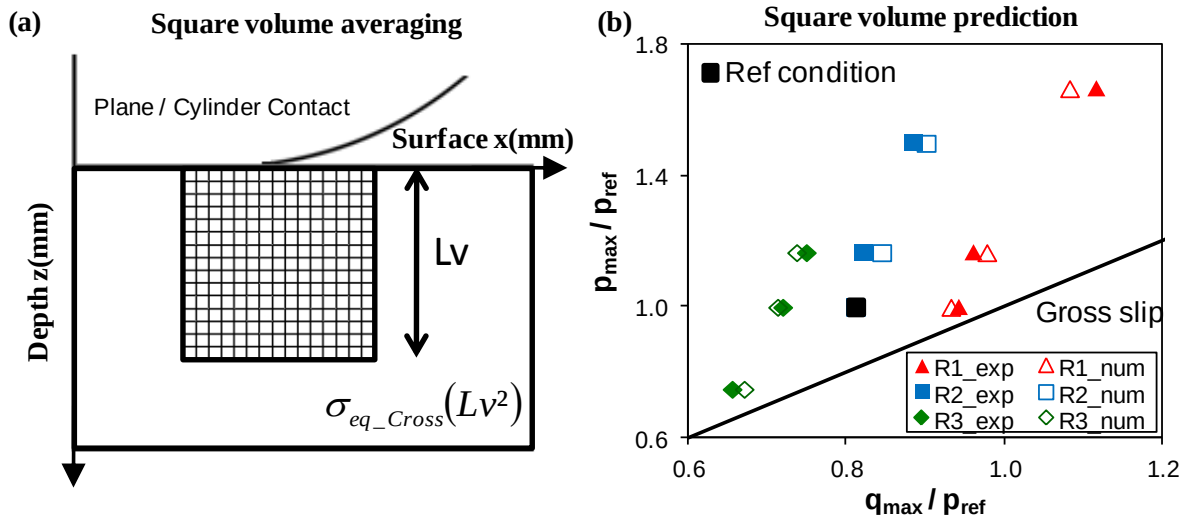

Fig. 11. (a) Numerical square volume averaging approach scheme and (b) shear threshold predicted by the non-local approach.

To quantify the error of prediction for each studied configuration, the following error index is computed:

$$E(\%) = 100 * \frac{\sum_i \left\| \frac{q_{th\_num(i)} - q_{th\_exp(i)}}{q_{th\_exp(i)}} \right\|}{n_i} \qquad (19)$$

The corresponding data are compiled in Table 3. The comparison with the local stress analysis clearly underlines the gain in terms of stability for prediction of the crack nucleation risk. The E(%) are systematically lower than 7.6%, whereas the mean value $\overline{E(\%)}$, computed from the studied condition, gives 3.1%, which is significantly smaller than the value obtained using the local stress analysis (29.1%). The crack boundary slopes are very close to the ones obtained experimentally. It is already possible to conclude that a constant volume averaging strategy is able to predict the nucleation threshold. The gap between each computed border seems equal to the experimental one. Thus, the constant volume averaging model can reflect the shear threshold increase for smaller contact radii.

9.2. Critical distance

An alternative strategy introduced by Araújo and al. for fretting cracking problems considers the stress at a critical distance below the point maximal of surface stress [22]. This strategy is presently adopted by identifying the critical Lc from which the crack nucleation related to the reference conditions (R_{ref}, p_{ref}, $qmax_{ref}$) is computed.

$$\sigma_{eq\_Cross}(Lc) = \tau_{d\_10^{-5}} \qquad (20)$$

The Lc parameter is set to 17 µm. This value is assumed constant and applied to predict the crack nucleation of each condition studied. Again the comparison with the experimental threshold leads to a very good correlation. The corresponding E(%) values are systematically lower than 7.7%, and the mean value $\overline{E(\%)}$, equal to 3.1%, which suggests that this basic non-local approach, like the square volume averaging approach, provides a very good estimation of the cracking risk. A very large spectrum of contact pressures and contact radii has been investigated.

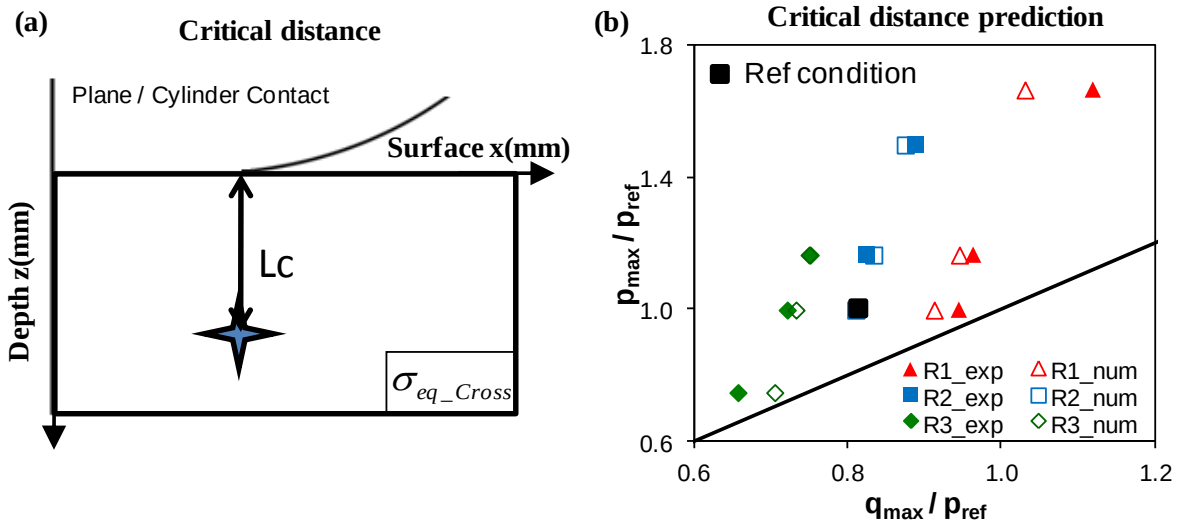

Fig. 12. (a) Diagram of critical distance criterion method and (b) numerical fretting map by the critical distance criterion.

9.3. Weighted function approach

The last strategy applied to consider the stress gradient effect is based on the Papadopoulos approach, using the stress gradient value in the Papadopoulos criterion equation. The gradient of a scalar value X = *f*(x, y, z) is defined by:

$$\|\nabla X\| = \sqrt{\left(\frac{\partial X}{\partial x}\right)^2 + \left(\frac{\partial X}{\partial y}\right)^2 + \left(\frac{\partial X}{\partial z}\right)^2} \qquad (21)$$

The Crossland stress value computed using local stress analysis is weighted by a coefficient *w*, which is function of the gradient of the hydrostatic pressure around the nucleated crack.

$$\sigma_{eq\_Cross}(w) = \left(\sqrt{J_{2,a}} + \alpha\sigma_{H,\max}\right) * w \qquad (22)$$

with:

$$w = 1 - k * \overline{\|\nabla\sigma_{h,\max}\|} \qquad (23)$$

with $\overline{\|\nabla\sigma_{h,\max}\|}$ the mean value of the gradient of the hydrostatic pressure. This mean value is computed over a square volume where the length is the threshold length Lp_{th}.

$$\overline{\left\|\nabla\sigma_{H,\max}\right\|} = \frac{1}{S}\int\int_{S}\left\|\nabla\sigma_{H,\max}\right\|.dS \qquad (24)$$

The k variable is identified from the reference test conditions (R_{ref}, p_{ref}, $qmax_{ref}$) by verifying the following relationship:

$$1 - k * \overline{\left\|\nabla\sigma_{h,\max}\right\|}_{ref} = \frac{\tau_{d\_10^{-5}}}{\sigma_{eq\_Cross\_ref}} \qquad (25)$$

$$k = \frac{1}{\overline{\left\|\nabla\sigma_{h,\max}\right\|}_{ref}} * \left(1 - \frac{\tau_{d\_10^{-5}}}{\sigma_{eq\_Cross\_ref}}\right) \qquad (26)$$

For the reference conditions investigated, we found k=8.596*10^{-5}. The w function is therefore characterized by a straight line starting from 1 when $\overline{\left\|\nabla\sigma_{h,\max}\right\|} = 0$ (i.e. non stress gradient condition) and passing through the reference point ($\overline{\left\|\nabla\sigma_{h,\max}\right\|}_{ref}$, $\tau_{d\_10^{-5}} / \sigma_{ec\_Cross\_ref}$).

To validate this linear assumption, all the corresponding ($\overline{\left\|\nabla\sigma_{h,\max}\right\|}$, $w_{\exp} = \tau_{d\_10^{-5}} / \sigma_{ec\_Cross}$) couples related to each set of test conditions are compared in Fig. 14b. All the points are aligned along the reference linear approximation. This a posteriori demonstrates the stability of the given linear dependency of the weighted function *w* as a function of the mean of the hydrostatic pressure stress gradient.

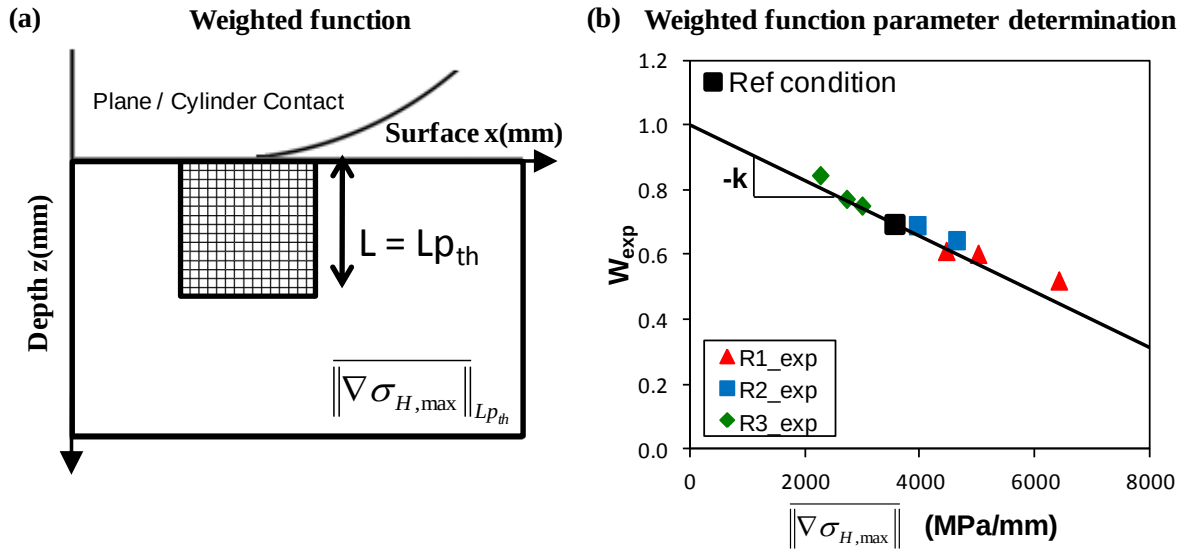

Fig. 13. (a) Mean hydrostatic pressure gradient computation and (b) determination of the k parameter used in the weighted function.

Like for the square averaging or critical distance methods, the experimental and predicted crack nucleation limits are compared in the (p_{max} vs. q_{max}) chart.

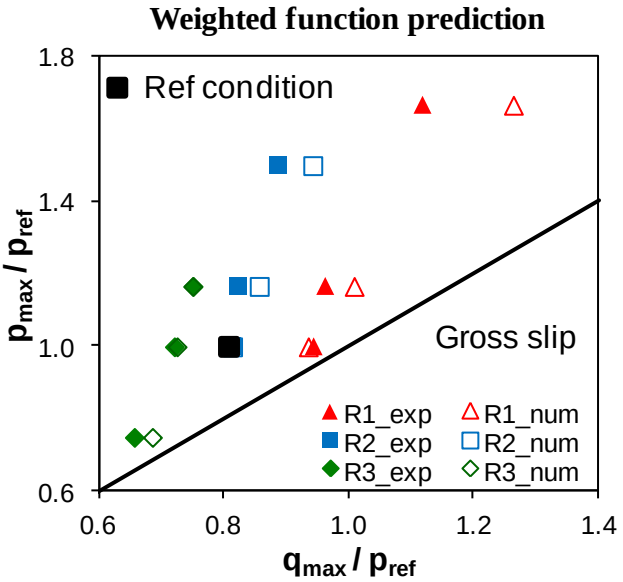

Fig. 14. Numerical fretting map using the weighted function approach

The errors between experimental and predicted values are very small, systematically smaller than 12.8% (Table 3). The computed mean value $\overline{E(\%)}$ is 4.2%, equivalent to that given by the former square averaging and critical distance approaches.

9.4. Synthesis

Charts ($\sqrt{J_{2a}}$ vs. $\sigma_{H,\max}$) which compare the various local and non local fatigue approaches clearly underline that a local approach is not suitable to predict the crack nucleation risk induced by fretting.

The comparison between the non-local fatigue approaches (Table 3, Fig. 16) suggests that whatever the approach, similar results are obtained. All these models provide accurate predictions with a mean index error value $\overline{E(\%)}$ lower than 4.2%.

The local description leads to a very large divergence from the predictions, and the prediction systematically overestimates the cracking risk.

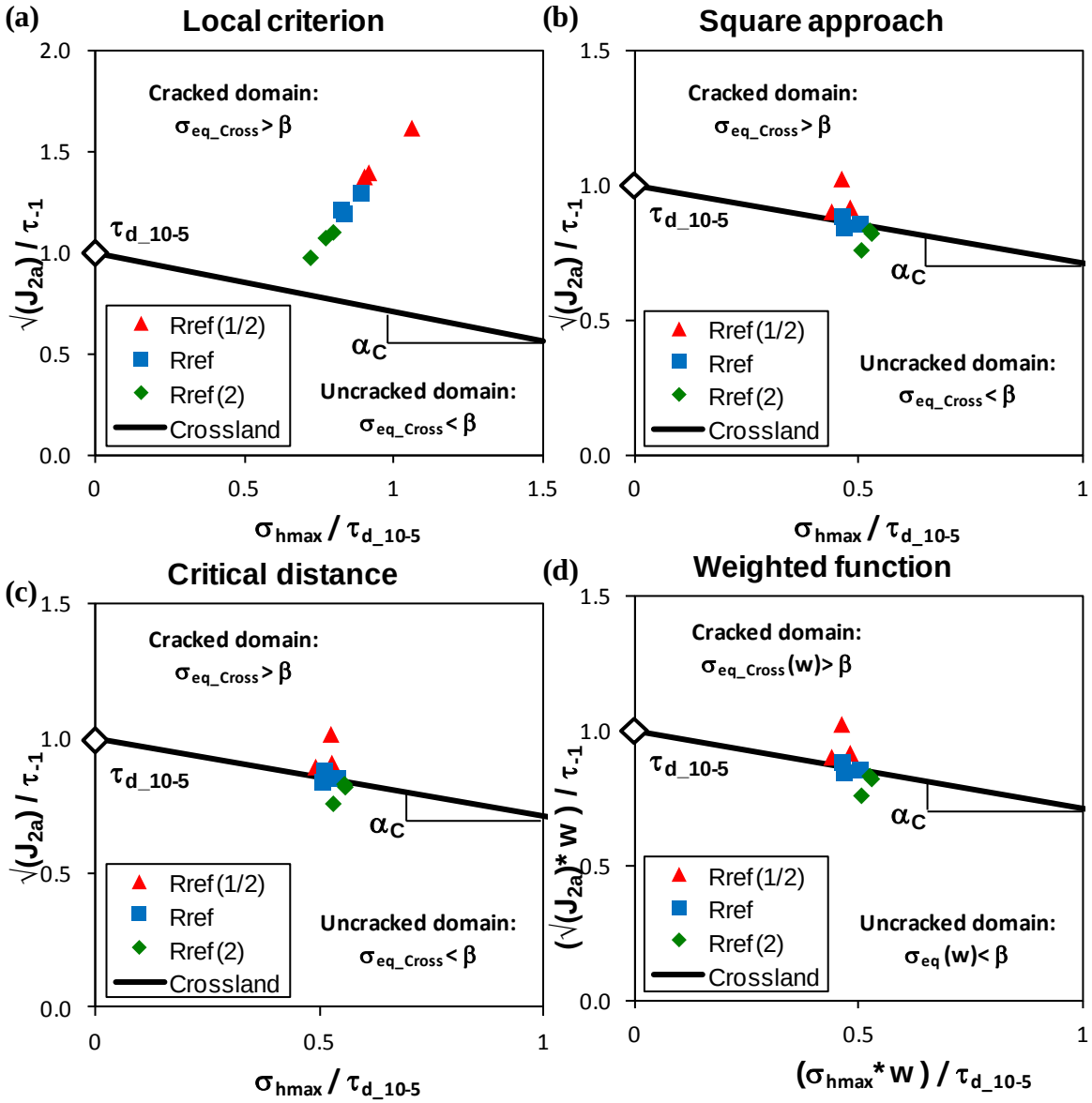

Fig. 15. ($\sqrt{J_{2a}}$ - $\sigma_{H,\max}$) charts: (a) local stress analysis, (b) square volume averaging, (c) critical distance and (d) weighted function.

The studied non local approaches (square volume averaging, critical distance and weighted function) display a very good correlation. All the predictions are aligned along the theoretical boundary.

The weighted function approach is quite complex to apply and does not significantly increase the accuracy of the prediction. Therefore the critical distance or the square volume averaging methods will be preferred regarding the computing time. The critical distance method appears to be the most pertinent model. It requires a single stress analysis at a given critical distance below the "hot point" (i.e., contact border |X|=a). However, to be transposed to industrial computation, the normal of the surface must thus be determined in order to locate the point at which the fatigue analysis must be done. The square volume averaging strategy performs the fatigue analysis at several points, at least 9 points to establish the averaged volume. However this approach does not require establishing the surface normal. It is therefore easier to apply using systematic FEM computation techniques. This is why this approach is currently adopted in engineering design models. Our current research work confirms that this approach is

appropriate for fretting cracking problems, and there is no need to implement more complex approaches like weighted function analysis to improve the accuracy of predictions, at least for the conditions and material. Besides, the constant square volume averaging criterion is based on a stress homogenization over a grain surface, which is more consistent with the physical description of the cracking process.

Table 3
Error between experimental results and predicted thresholds for each approach in the study.

Contact radii	p_{max}/p_{ref}	E(%) Local stress analysis	E(%) Square volume Lv=37µm	E(%) Critical distance Lc=17µm	E(%) Weighted function
$R_{ref(2)}$	0.75	14.6	7.6	7.7	4.3
	1.00	21.3	1.9	2.0	0.5
	1.17	24.0	0.2	0.2	0.2
R_{ref}	1.00	27.9	-	-	-
	1.17	28.3	1.5	1.5	3.7
	1.50	32.2	0.9	1.1	6.1
$R_{ref(1/2)}$	1.00	35.0	3.3	3.1	1.1
	1.17	35.4	1.6	1.5	4.6
	1.67	42.8	7.6	7.6	12.8
$\overline{E(\%)}$	-	29.1	3.1	3.1	4.2

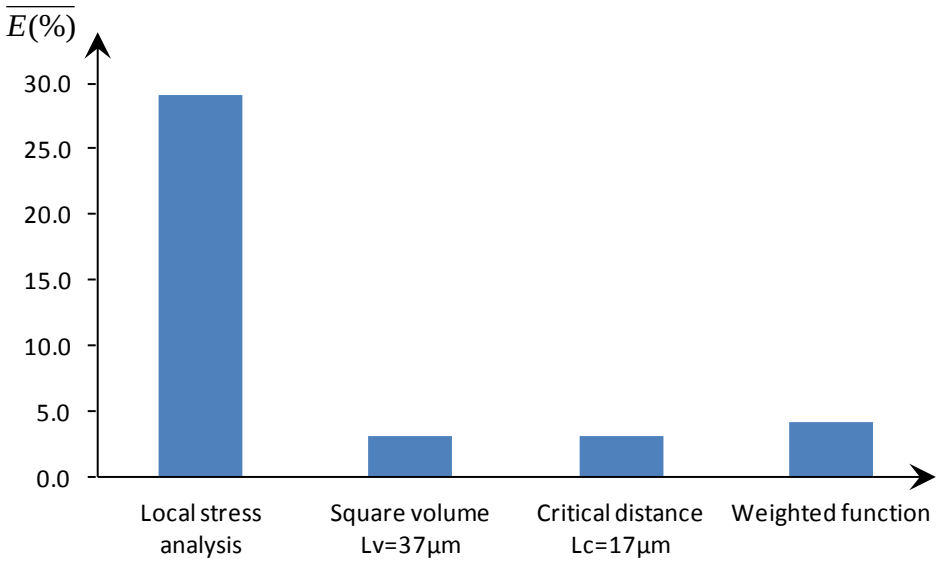

Fig. 16. Mean error index values for the various numerical methods.

10. Conclusion

A dedicated analysis has been performed to quantify the crack nucleation risk introduced by plain fretting loading focusing on stress gradient effects. The following conclusions have been derived:

- At the contact border, the zone of the maximum cracking risk, the stress loading path is proportional, which infers that all the conventional multiaxial criteria lead to equivalent predictions. Therefore the simplest approach, Crossland's, is preferred.

- The stress gradient imposed below the surface plays a critical impact on the cracking prediction. For a given pressure, the larger the contact area, the higher the quantity of material affected by the maximum stress and therefore the higher the cracking risk. To efficiently predict the cracking risk, a non-local multiaxial fatigue approach must be adopted.

- The comparison between various non local approaches (i.e., square averaging, critical distance and weighted function) transposed to the Crossland criterion leads to equivalent predictions. For practical reasons, the square averaging approach is preferred.

11. Acknowledgements

This research is financially supported by SNECMA. The authors wish to thank R. Amargier, J. Mériaux, and N. Serres for their remarks on and support of this work.

12. References

[1] A. Hutson, H. Lee, and S. Mall, "Effect of dissimilar metals on fretting fatigue behavior of Ti–6Al–4V," *Tribology International*, vol. 39, no. 10, pp. 1187-1196, Oct. 2006.

[2] S. Fouvry, P. Duó, and P. Perruchaut, "A quantitative approach of Ti–6Al–4V fretting damage: friction, wear and crack nucleation," *Wear*, vol. 257, no. 9–10, pp. 916-929, Nov. 2004.

[3] D. Nowell and J. A. Araújo, "The effect of rapidly varying contact stress fields on fretting fatigue," *International Journal of Fatigue*, vol. 24, pp. 763-775, 2002.

[4] R. Amargier, S. Fouvry, L. Chambon, C. Schwob, and C. Poupon, "Stress gradient effect on crack initiation in fretting using a multiaxial fatigue framework," *International Journal of Fatigue*, vol. 32, no. 12, pp. 1904-1912, Dec. 2010.

[5] C. Navarro, S. Munoz, and J. Dominguez, "On the use of multiaxial fatigue criteria for fretting fatigue life assessment," *International Journal of Fatigue*, vol. 30, no. 1, pp. 32-44, Jan. 2008.

[6] D. Nowell, D. Dini, and D. A. Hills, "Recent developments in the understanding of fretting fatigue," *Engineering Fracture Mechanics*, vol. 73, no. 2, pp. 207-222, Jan. 2006.

[7] C. Petiot, L. Vincent, K. Dang Van, N. Maouche, J. Foulquier, and B. Journet, "An analysis of fretting-fatigue failure combined with numerical calculations to predict crack nucleation," *Wear*, vol. 183, pp. 101-111, 1995.

[8] I. V. Papadopoulos, "A high-cycle fatigue criterion applied in biaxial and triaxial out-of-phase stress conditions," *Fatigue & Fracture of Engineering Materials and Structures*, vol. 18, no. 1, pp. 79-91, Jan. 1995.

[9] S. Fouvry, P. Kapsa, and L. Vincent, “Quantification of fretting damage,” *Wear*, vol. 200, pp. 186-205, 1996.

[10] M. P. Szolwinski and T. N. Farris, “Mechanics of fretting fatigue crack formation,” *Wear*, vol. 198, pp. 93-107, 1996.

[11] I. V. Papadopoulos, “Long life fatigue under multiaxial loading,” *International Journal of Fatigue*, vol. 23, no. 10, pp. 839-849, Nov. 2001.

[12] B. Crossland, “Effect of large hydrostatic pressures on the torsional fatigue strenght of an alloy steel,” in *Proceedings of the international conference on fatigue of metals*, 1956, pp. 138-149.

[13] S. Fouvry, P. Kapsa, and L. Vincent, “A Multiaxial Fatigue Analysis of Fretting Contact Taking Into Account the Size Effect,” in *ASTM*, 2000, pp. 167-182.

[14] J. A. Araújo, L. Susmel, D. Taylor, J. Ferro, and E. Mamiya, “On the use of the Theory of Critical Distances and the Modified Wöhler Curve Method to estimate fretting fatigue strength of cylindrical contacts,” *International Journal of Fatigue*, vol. 29, no. 1, pp. 95-107, Jan. 2007.

[15] H. Proudhon, S. Fouvry, and G. Yantio, “Determination and prediction of the fretting crack initiation: introduction of the (P, Q, N) representation and definition of a variable process volume,” *International Journal of Fatigue*, vol. 28, no. 7, pp. 707-713, Jul. 2006.

[16] K. Nakazawa, N. Maruyama, and T. Hanawa, “Effect of contact pressure on fretting fatigue of austenitic stainless steel,” *Tribology International*, vol. 36, no. 2, pp. 79-85, Feb. 2003.

[17] S. Fouvry and K. Kubiak, “Introduction of a fretting-fatigue mapping concept: Development of a dual crack nucleation – crack propagation approach to formalize fretting-fatigue damage,” *International Journal of Fatigue*, vol. 31, no. 2, pp. 250-262, Feb. 2009.

[18] J. J. Madge, S. B. Leen, and P. H. Shipway, “The critical role of fretting wear in the analysis of fretting fatigue,” *Wear*, vol. 263, no. 1–6, pp. 542-551, Sep. 2007.

[19] M. H. Zhu, Z. R. Zhou, P. Kapsa, and L. Vincent, “Radial fretting fatigue damage of surface coatings,” *Wear*, vol. 250, no. 1–12, pp. 650-657, Oct. 2001.

[20] I. V. Papadopoulos, “Invariant formulation of a gradient dependent multiaxial high-cycle fatigue criterion,” *Engineering Fracture Mechanics*, vol. 55, no. 4, pp. 513-528, 1996.

[21] S. Fouvry, P. Kapsa, F. Sidorof, and L. Vincent, “Identification of the characteristic length scale for fatigue cracking in fretting contacts.,” in *J. Phys IV France*, 1998, pp. 159-166.

[22] J. A. Araújo, L. Susmel, D. Taylor, J. C. T. Ferro, and J. L. A. Ferreira, “On the prediction of high-cycle fretting fatigue strength: Theory of critical distances vs. hot-spot approach,” *Engineering Fracture Mechanics*, vol. 75, no. 7, pp. 1763-1778, May 2008.

[23] H. Proudhon, S. Fouvry, and J. Buffiere, “A fretting crack initiation prediction taking into account the surface roughness and the crack nucleation process volume,” *International Journal of Fatigue*, vol. 27, no. 5, pp. 569-579, May 2005.

[24] R. D. Mindlin and H. Deresiewiez, “Elastic spheres in contact under varying oblique forces,” *Journal of Apple Mech*, vol. 20, pp. 327-344, 1953.

[25] C. Cattenao, “Sul contatto di due corpi elastici: distribuzionelocaledeglisforzi,” *Rendiconti dell’ Accademia dei Lincei*, vol. 27, pp. 343-8,434-6,474-8, 1938.

[26] K. L. Johnson, *Contact mechanics*. 1985.

[27] J. Lu, “Fatigue des alliages ferreux : définitions et diagrammes,”*Techniques de l’ingénieur*. pp. 1-14.

[28] I. V. Papadopoulos, P. Davoli, C. Gorla, M. Filippini, and A. Bernasconi, “A comparative study of multiaxial high-cycle fatigue criteria for metals,” *International Journal of Fatigue*, vol. 19, no. 3, pp. 219-235, 1997.

[29] S. Fouvry and K. Kubiak, “Development of a fretting–fatigue mapping concept: The effect of material properties and surface treatments,” *Wear*, vol. 267, no. 12, pp. 2186-2199, Dec. 2009.

[30] M. Ciavarella, “The generalized catteneo partial slip plane contact problem. I-Theroy,” *International Journal of Solids and Structures*, vol. 35, no. 18, pp. 2349-2362, 1998.

[31] M. Ciavarella, “The gerneralized cattaneo partial slip plane contact problem. II-Examples,” *International Journal of Solids and Structures*, vol. 35, no. 18, pp. 2363-2378, 1998.